Ultrafast Dynamics of Single-Walled Carbon Nanotubes Dispersed in Polymer Films

David J. Styers-Barnett,[†] Stephen P. Ellison,[†] Cheol Park,[‡] Kristopher E. Wise,[‡] and John M. Papanikolas*,[†]

Department of Chemistry, University of North Carolina, Chapel Hill, North Carolina 27599-3290, and National Institute of Aerospace, NASA Langley Research Center, MS 226, Hampton, Virginia 23681-2199

Received: November 24, 2004

Wavelength-resolved femtosecond transient absorption spectroscopy is used to follow the electronic dynamics of single-walled carbon nanotubes in polymers following visible photoexcitation. Electron−hole (e−h) pairs give rise to sharp features in the transient spectra that decay in amplitude and exhibit rapid spectral shifts. The decay reflects (e−h) recombination on both short (1.3 ps) and long (35 ps) time scales. Transient spectra also exhibit a broad photobleach at early times that arises from the cooling of a hot electron gas created via excitation at the red edge of a π-plasmon band.

I. Introduction

Single-walled carbon nanotubes (SWNTs) offer a unique environment in which to study the electronic dynamics of extended systems. Nanotube samples contain both semiconducting and metallic tubes (typically 2:1 ratio), and accordingly, a variety of excitation and relaxation processes will contribute to the observed dynamics. In the case of the metallic tubes, visible irradiation can excite a plasmon resonance,[1] which coherently drives the π electrons near the Fermi level. This produces a hot electron gas that thermally relaxes via electron−electron and electron−phonon scattering. In addition to plasmon excitations, electron−hole (e−h) pairs are produced in nanotubes when an electron is promoted from the valence band to the conduction band (Figure 1, right) following the absorption of a photon. In this optically prepared state, the electron and hole are most likely bound to each other by their mutual electrostatic attraction, forming excitons.[2−4] Analogous to inorganic semiconductors, one might anticipate a variety of dynamic processes following exciton formation, including geminate recombination, dissociation into free carriers followed by nongeminate recombination, and biexciton annihilation processes.

While there has been a great deal of work focusing on the mechanical, electronic, and steady-state optical properties of SWNTs,[1−12] the efforts[13−25] performed on ultrafast time scales have not provided a definitive picture of the excited-state relaxation dynamics. Experiments performed on SWNT mats (i.e., buckypaper) and nanotubes on glass substrates report different time scales for excited-state decay; a fast component on a 100−200 fs time scale, a slower ∼1 ps time component,[18−22] and in a few studies on isolated SWNTs in micelles, a long (>100 ps) decay has been reported as well.[13,14,18,25] These observations have been attributed to a range of dynamic processes including exciton recombination, plasmon relaxation, electron cooling, and radiative relaxation. Differences between
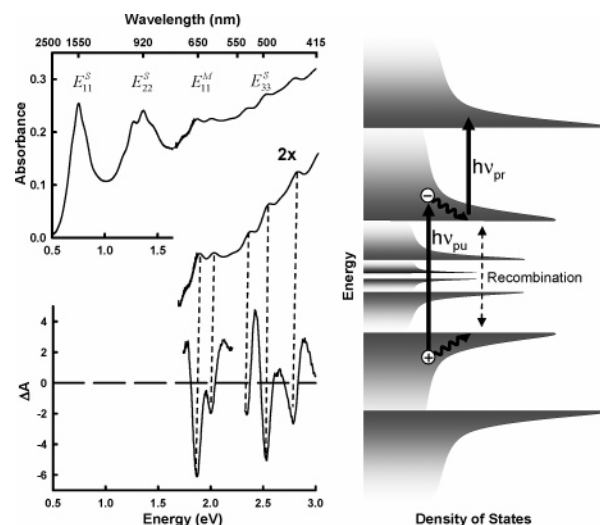
Figure 1. (Right) illustration depicting the density of SWNT energy states for valence and conduction bands of semiconducting SWNTs. There is an increase in the density of states near the band edges termed the van-Hove singularities (vHs). Photon absorption from the pump pulse ($h\nu_{pump}$) results in the promotion of an electron to the conduction band, resulting in an electron−hole (e−h) pair. (Left) ground-state absorption spectrum of the SWNT/CP2 polymer composite displayed in the upper panel, and the transient absorption spectrum observed 800 fs after 550 nm excitation shown in the lower panel. The inset is the ground-state spectrum magnified by a factor of 2. The peak labels E_{11}^S, E_{22}^S, E_{33}^S indicate the transition between the first, second, and third pairs of van Hove singularities in semiconducting tubes while E_{11}^M corresponds to the first transition in metallic tubes.

isolated[13−18] and bundled[17−24] systems could stem from a lack of multitube processes in isolated samples; thus direct comparisons between the two may not be appropriate.

Because these systems were probed using single-wavelength detection, assignment of the kinetic components to a specific dynamic process was difficult. Single-wavelength methods provide a limited view of the excited-state spectroscopy, and

* Corresponding author. E-mail address: John_Papanikolas@unc.edu.
† University of North Carolina.
‡ NASA Langley Research Center.

in general, it is impossible to determine whether a multiexponential decay is the result of a *decrease* in the amplitude of an absorption band or a *shift* in its position. Using single wavelength techniques, most ultrafast studies of SWNT bundles[17;18;22−24] have assigned excited-state kinetics to *intraband* scattering processes (electron−electron, electron−phonon, etc.) occurring on time scales ranging from 0.2 to 1 ps. This designation is counter to recent publications[20;21] that link the observed kinetics to *interband* electron−hole recombination processes, showing that a definitive assignment from single-wavelength studies has remained elusive.

Our experimental methodology differs from these previous studies in one major respect: we are able to examine the evolution of the transient *spectrum*, not just single wavelength kinetics. The use of spectrally resolved transient absorption (TA) spectroscopy allows us to identify *both* interband and intraband dynamics. We observe a broad photobleach as well as narrow spectral features (absorptions and bleaches) in the nanotube spectra, which reflect intraband and interband processes, respectively. The broad photobleach decays with a 150 fs time constant and based on power dependence studies, we assign it to plasmon relaxation in the metallic tubes. The narrow features decay in amplitude and exhibit rapid spectral shifts. The intensity decay reflects (e−h) recombination, which is observed to occur with both fast (1.3 ps) and slow (35 ps) time components, while the absorption features blue shift during the first 25 ps after photoexcitation. Given the complex nature of the excited-state dynamics, the ability to examine *transient spectra* provides a clear advantage over single-wavelength detection.

II. Experimental Methods and Results

This paper focuses on nanotube bundles embedded in a polymer matrix. The sample is a 100 μm thick film of 0.1% (by weight) laser ablated SWNTs in CP2, a colorless polyimide (**1**).

$$-\left(N\underset{O}{\overset{O}{\Vert}}...\underset{O}{\overset{O}{\Vert}}N-\bigcirc-O-\bigcirc-O-\bigcirc\right)- \qquad (1)$$
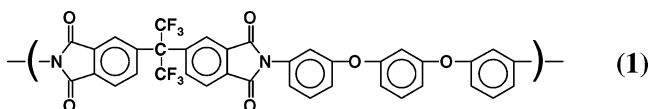
The diameter distribution of the individual nanotubes in the bundles is 0.8−1.1 nm. In general, bundle size is dependent on a number of factors such as the production method (laser ablation, HiPco, etc.), the nature of the polymer matrix, and the method of dispersion. Electrical percolation and various probe microscopies (TEM, AFM, and MFM) suggest that the NT bundles in these samples are fairly small, on the order of 10−20 tubes, indicating that the polymer induces a significant degree of debundling.

The ground state absorption spectrum of the SWNT/CP2 composite is displayed in the top left panel of Figure 1. The polyimide matrix is transparent to the red of 400 nm; therefore the carbon nanotubes are the only contributors to the observed absorption in this region of the spectrum. The absorption consists of a series of features (labeled E_{11}^S through E_{33}^S) arising from interband $\pi\pi^*$ transitions. These transitions are enhanced by an increase in the density of states that results from a flattening of the bands near the edges of the Brillouin zone, i.e. the van Hove singularities (vHs).[2] Since both the semiconducting and metallic tubes contain singularities, photoexcitation produces (e−h) pairs in all nanotubes regardless of chirality. Closer inspection reveals that the absorptions are inhomogeneously broadened by a number of smaller features. These most likely arise from spectral congestion (due to transitions between
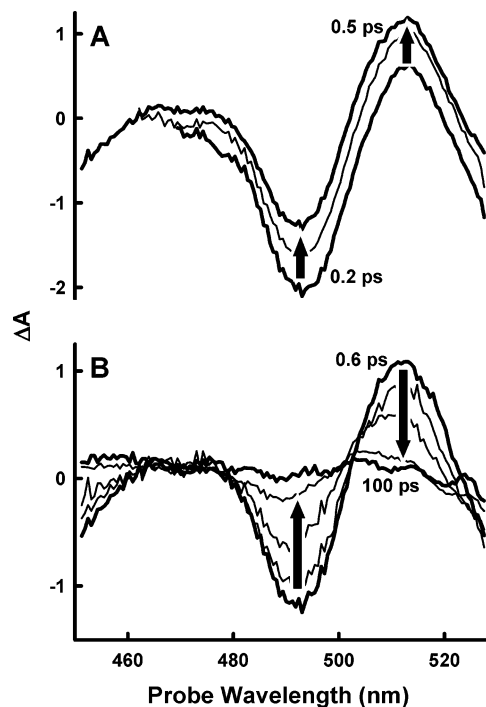

Figure 2. Transient absorption spectra of SWNT/CP2 composite obtained at different times after photoexcitation. The spectra are divided into two categories. (A) shows the spectral evolution during the first 500 fs. During this time an increase in the TA signal is observed at all wavelengths. Spectra shown are 200, 300, and 500 fs after excitation. (B) shows the spectral evolution after 500 fs. During this time the absorption and bleach signals decay in amplitude (arrows), reflecting (e−h) recombination, and there is a blue shift (from 512 to 505 nm) of the excited-state absorption feature. Five spectra (0.6, 1, 2, 25, and 100 ps) are shown.

overlapping subbands), as well as a distribution of transition frequencies resulting from the presence of NTs with different diameters and chiral wrappings. The absorptions due to these discrete transitions are superimposed on top of a large background assigned to the red tail of a broad π plasmon resonance[1] that peaks at ~6 eV. This absorption, which is analogous to the surface plasmon excitation observed in metallic nanoparticles,[26] corresponds to the optically driven coherent oscillation of electrons near the Fermi level.[27]

The photoinduced dynamics are studied using femtosecond TA spectroscopy. The details regarding the experimental setup have been discussed elsewhere.[28] The transient absorption spectrum of the SWNT/CP2 composite obtained 800 fs after 550 nm photoexcitation (150 fs pulse duration, 1 μJ/pulse; 300 μm diameter) is displayed from 390 to 715 nm in the lower left panel of Figure 1. Excitation at this energy lies between the first metallic transition, E_{11}^M, and the third semiconducting, E_{33}^S, so we anticipate excited state formation in both types of SWNT. The spectrum shows a series of both positive and negative going features. Negative features signify enhanced transmission of the probe beam upon excitation. Each negative peak in the TA spectrum corresponds to a transition in the ground state absorption spectrum (Figure 1), and therefore they are assigned to ground state photobleaching. The positive signals are attributed to excited-state absorptions, and like the bleaches, the absorptions are spectrally narrow, suggesting that they represent transitions to vHs at higher energy.

A portion of the transient spectrum is shown in Figure 2 for a series of pump−probe delays. At very early times (<500 fs, Figure 2A), there is little or no change in the shape (i.e., position, peak-to-peak amplitude, and width) of the spectra. There is,

Letters

*J. Phys. Chem. A, Vol. 109, No. 2, 2005* **291**
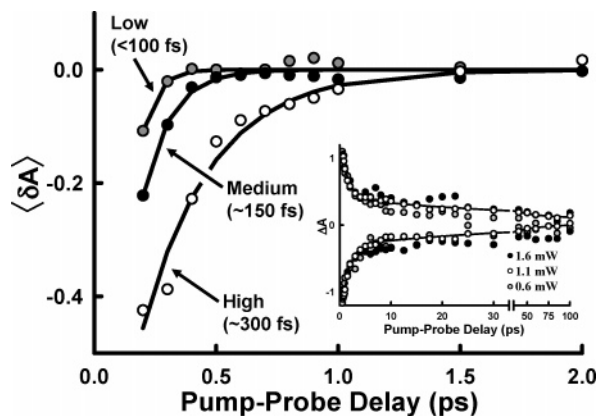
Figure 3. Power dependence of the SWNT plasmon signal. The plot shows the average of the TA spectrum from 475 to 525 nm, $\langle \delta A \rangle$, as a function of pump−probe delay for three excitation intensities; 1.6 mJ/pulse (white circles), 1 mJ/pulse (black circles), and 0.6 mJ/pulse (gray circles). See the text for a full description of this quantity. As pump intensity increases, the decay time for the plasmon lengthens from <100 to 300 fs. Lines in the plot are single-exponential fits to each data set. The inset shows the power dependence out to 100 ps for the absorption and bleach decays for all powers studied. Each curve has identical biphasic relaxation dynamics for exciton recombination.

however, an increase in the TA signal observed at all wavelengths that begins upon excitation and is finished by 500 fs. The upward change suggests the presence of a broad transient feature, corresponding to either a rapidly decaying bleach or the appearance of an excited state absorption. The evolution of this element appears to be independent of changes in the other spectral features, and therefore it does not seem to result from the flow of population from one excited state to another. That is, there appear to be at least two, instantaneously formed, independently evolving excited states. Furthermore, if it were excited-state absorption, then we should observe a broad absorption band that persists at long pump−probe delays and/ or evidence for its decay. We observe neither, and for this reason we associate this feature with a broad photobleach that decays to zero with a lifetime of ∼150 fs. This assignment is consistent with a recent report of a broad photobleach in the transient spectra of isolated SWNT in micelles.[25] The extended spectral range and rapid relaxation suggest the transition corresponds to the π plasmon absorption in metallic NTs.

The dependence of the intensity of this broad photobleach and its associated kinetics on excitation fluence provides strong support to the plasmon relaxation assignment. Shown in Figure 3 is the average transient absorption signal from 475 to 525 nm divided by the amplitude difference of the narrow features, as a function of pump probe delay:

$$\langle \delta A \rangle = \frac{\langle \Delta A \rangle_\lambda}{\Delta A_0(510) - \Delta A_0(490)} \quad (1)$$

where $\Delta A_0(\lambda)$ is the initial TA signal at a given wavelength, λ. The denominator allows us to plot the spectral offset as a percentage of the peak-to-peak amplitude of the signal. By displaying this quantity, we separate out the evolution of the broad photobleach from that of the narrow features. As the power increases, the magnitude and decay time of the bleach increase. The time constant ranges from instrument response limited to ∼300 fs at the highest laser power. Link and El-Sayed observed[27] a slower electron−electron cooling rate with increased excitation intensity in their power dependence studies of plasmon relaxation in gold nanoparticles. Although our power dependence trend is consistent with their observations, our
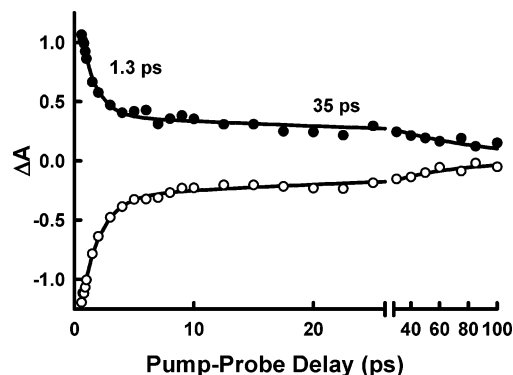
Figure 4. Transient decay of the photobleach monitored at 492 nm (open circles) and the photoabsorption monitored at the peak maximum (filled circles). The transients exhibit biexponetial decay kinetics with fast and slow time components of 1.3 and 35 ps, respectively. The solid lines represent a simultaneous fit of both signals. For the fit, the time constants are held constant, but the amplitudes are variable.

samples show faster plasmon relaxation than the gold nanoparticles. This may be expected given that SWNT can rapidly dissipate energy along the length of the tube, or perhaps even across tubes in a bundle.

On longer time scales (>500 fs, Figure 2B) we observed evolution in the amplitude and shape of the narrower features. The most prominent change is associated with the decay of the photobleach and excited-state absorption. Figure 4 shows the peak amplitudes as a function of pump−probe delay for both components. Both exhibit a fast component of ∼1.3 ps, as well as a slower 35 ps component. Because the absorption and the bleach decay on identical time scales, they must reflect the same dynamic process, namely (e−h) recombination.

The observation of two time scales in these transient spectra suggests the presence of two different relaxation pathways. Exciton−exciton annihilation could lead to this type of behavior. A clear indication of this would be intensity-dependent kinetics. Examination of the long-time signals at a range of excitation intensities (Figure 3, inset) shows that power dependence is not observed in the recombination kinetics. Indeed, for the power range investigated, only the plasmon decay shows a power-dependent rate. Although we do not see such effects, Fleming and co-workers[13] reported intensity-dependent transient absorption signals of micelle encapsulated SWNTs. Another possibility is that the fast component reflects geminate (e−h) recombination, while the slow component shows (e−h) pair dissociation followed by diffusion and eventual recombination, either geminate or nongeminate. The TA spectra observed at long times appear to indicate the presence of weak residual structure that persists throughout the time scale of our experiment. This could be evidence of (e−h) dissociation, which lends support to this hypothesis.

We also observe a time-dependent blue shift in the absorption feature that takes place during the first 25 ps after photoexcitation. At 600 fs the peak is centered at 512 nm, and by 25 ps, the maximum has completed its shift to ∼505 nm. There are several possible explanations for this time-dependent blue shift. For example, the cooling of the charge carriers prior to recombination would *increase* the transition energy to a higher energy band, and thus shift the excited-state absorption to the blue. Alternatively, flow of the excited-state energy from one tube to another in bundles could correspond to the blue shift. Experiments on nanotubes embedded in other polymers show a spectral shift with the same magnitude and kinetic rates,[29] suggesting that this process, whatever the origin, is intrinsic to the nanotubes.

III. Conclusion

Our results differ from previous reports on the ultrafast dynamics of SWNTs in several ways. First, our data clearly show the presence of biphasic exciton recombination kinetics with both fast (1.3 ps) and slow (35 ps) time components, whereas prior studies[20,21] find only a single fast decay with a 0.7−1 ps recombination time. The observation of biexponential band-edge recombination kinetics indicates the presence of multiple relaxation pathways following photoexcitation. Second, we report a clear time-dependent blue shift in the absorption features during the first 25 ps after excitation. This could reflect the carrier relaxation to the band edge, or an electrostatic interaction between the (e−h) pair and the surrounding environment. A final observation made clear by wavelength-resolved detection is the broad photobleach that has rapid kinetic decay (150 fs). Its spectral shape and power dependence imply that it corresponds to plasmon relaxation via electron−electron and electron−phonon scattering processes. It is interesting to note that other papers do mention fast (150 fs) kinetic components, but they do not connect them with broad spectral features. Clearly there are many different relaxation pathways in SWNT that could contribute to the spectroscopic signals at any given probe wavelength. Our experiments have identified at least *three* different kinetic processes that simultaneously contribute to the observed signals. By measuring the *transient spectrum* we can distinguish between these contributions and thereby disentangle the dynamic processes.

References and Notes

(1) Bursill, L. A.; Stadelmann, P. A.; Peng, J. L.; Prawer, S. *Phys. Rev. B* **1994**, *49*, 2882−2887.

(2) Spataru, C. D.; Ismail-Beigi, S.; Benedict, L. X.; Louie, S. G. *Phys. Rev. Lett.* **2004**, *92*, 077402.

(3) Kane, C. L.; Mele, E. L. *Phys. Rev. Lett.* **2003**, *90*, 207401.

(4) Pedersen, T. G. *Phys. Rev. B* **2003**, *67*, 073401.

(5) Arnold, M. S.; Sharping, J. E.; Stupp, S. I.; Kumar, P.; Hersam, M. C. *Nano Lett.* **2003**, *3*, 1549−1554.

(6) O'Connell, M. J.; Bachilo, S. M.; Huffman, C. B.; Moore, V. C.; Strano, M. S.; Haroz, E. H.; Rialon, K. L.; Boul, P. J.; Noon, W. H.; Kittrell, C.; Ma, J.; Hauge, R. H.; Weisman, R. B.; Smalley, R. E. *Science* **2002**, *297*, 593−596.

(7) Knupfer, M.; Pichler, T.; Golden, M. S.; Fink, J.; Rinzler, A.; Smalley, R. E. *Carbon* **1999**, *37*, 733−738.

(8) Chiang, I. W.; Brinson, B. E.; Huang, A. Y.; Willis, P. A.; Bronikowski, M. J.; Margrave, J. L.; Smalley, R. E.; Hauge, R. H. *J. Phys. Chem. B* **2001**, *105*, 8297−8301.

(9) Lin, M. F.; Shung, W.-K. *Phys. Rev. B* **1994**, *50*, 17744−17747.

(10) Harris, P. J. F. *Carbon Nanotubes and Related Structures*; Cambridge University Press: Cambridge, 1999.

(11) Ouyang, M.; Huang, J. L.; Lieber, C. M. *Acc. Chem. Res.* **2002**, *35*, 1018−1025.

(12) Souza, A. G.; Jorio, A.; Dresselhaus, G.; Dresselhaus, M. S.; Saito, R.; Swan, A. K.; Unlu, M. S.; Goldberg, B. B.; Hafner, J. H.; Lieber, C. M.; Pimenta, M. A. *Phys. Rev. B* **2002**, *65*.

(13) Ma, Y.-Z.; Stenger, J.; Zimmermann, J.; Bachilo, S. M.; Smalley, R. E.; Weisman, R. B.; Fleming, G. R. *J. Chem. Phys.* **2004**, *120*, 3368−3373.

(14) Ostojic, G. N.; Zaric, S.; Kono, J.; Strano, M. S.; Moore, V. C.; Hauge, R. H.; Smalley, R. E. *Phys. Rev. Lett.* **2004**, *92*, 117402.

(15) Huxtable, S. T.; Cahill, D. G.; Shenogin, S.; Xue, L.; Ozisik, R.; Barone, P.; Usrey, M.; Strano, M. S.; Siddons, G.; Shim, M.; Keblinski, P. *Nature Mater.* **2003**, *2*, 731−734.

(16) Kono, J.; Ostojic, G. N.; Zaric, S.; Strano, M. S.; Moore, V. C.; Shaver, J.; Hauge, R. H.; Smalley, R. E. *Appl. Phys. A−Mater. Sci. Processing* **2004**, *78*, 1093−1098.

(17) Hagen, A.; Moos, G.; Talalaev, V.; Hertel, T. *Appl. Phys. A* **2004**, *78*, 1137−1145.

(18) Huang, L.; Pedrosa, H. N.; Krauss, T. D. *Phys. Rev. Lett.* **2004**, *93*, 017403.

(19) Lauret, J. S.; Voisin, C.; Cassabois, G.; Delalande, C.; Roussignol, P.; Jost, O.; Capes, L. *Phys. Rev. Lett.* **2003**, *90*.

(20) Lauret, J. S.; Voisin, C.; Cassabois, G.; Delalande, C.; Roussignol, P.; Capes, L.; Jost, O. *Physica E−Low-Dimensional Systems & Nanostructures* **2003**, *17*, 380−383.

(21) Korovyanko, O. J.; Sheng, C.-X.; Vardeny, Z. V.; Dalton, A. B.; Baughman R. H. *Phys. Rev. Lett.* **2004**, *92*, 017403.

(22) Hertel, T.; Fasel, R.; Moos, G. *Appl. Phys. A−Mater. Sci. Processing* **2002**, *75*, 449−465.

(23) Ichida, M.; Hamanaka, Y.; Kataura, H.; Achiba, Y.; Nakamura, A. *Phys. B−Condens. Matter (Amsterdam)* **2002**, *323*, 237−238.

(24) Hertel, T.; Moos, G. *Phys. Rev. Lett.* **2000**, *84*, 5002−5005.

(25) Nadtochenko, V. A.; Lobach, A. S.; Gostev, F. E.; Sarkisov, O. M.; Shcherbinin, D. O.; Obraztova, E. D. *JETP* **2004**, *80*, 176−180.

(26) Link, S.; Burda C.; Mohamed, M. B.; Nikoobakht, B.; El-Sayed, M. A. *Phys. Rev. B* **2000**, *61*, 6086−6090.

(27) Link, S.; El-Sayed, M. A. *J. Phys. Chem. B* **1999**, *103*, 8410−8426.

(28) Shaw, G. B.; Brown, C. L.; Papanikolas, J. M. *J. Phys. Chem. A* **2002**, *106*, 1483−1495.

(29) Styers-Barnett, D. J.; Park, C.; Wise, K. E.; Papanikolas, J. M. Manuscript in preparation.